nature climate change

LETTERS

https://doi.org/10.1038/s41558-019-0566-x

Indian Ocean warming can strengthen the Atlantic meridional overturning circulation

Shineng Hu[1*] and Alexey V. Fedorov[2,3]

The slowdown of the Atlantic meridional overturning circulation (AMOC)[1–3] and the accelerated warming of the tropical Indian Ocean (TIO)[4–6] are two robust features projected for anthropogenic greenhouse warming, affecting both regional and global climates[7,8]. Here we use coupled climate simulations to investigate a previously overlooked link between the two phenomena. We demonstrate that TIO warming reduces rainfall over the tropical Atlantic by strengthening the Walker circulation and increasing atmospheric vertical stability. The resultant ocean salinity increase intensifies the AMOC as salinity anomalies are advected to northern high latitudes. In addition, TIO warming enhances westerly winds over the subpolar North Atlantic, which helps to maintain the stronger AMOC. A TIO warming of 0.1 °C above the mean warming of tropical oceans intensifies the AMOC by ~1 Sv, leading to a stronger interhemispheric asymmetry and a northward shifted ITCZ. Thus, TIO warming could delay the AMOC weakening under greenhouse warming. Indeed, we find that the AMOC weakens more strongly or completely collapses if we suppress TIO warming under the doubled and quadrupled CO_2 scenarios. Simulations replicating the observed tropical ocean warming further confirm this TIO–AMOC link, suggesting that the observed TIO warming might be already playing a role in sustaining the AMOC.

The tropics influence global climate both directly and indirectly. A localized heating of the tropical atmosphere due to convective latent heat release can trigger atmospheric waves that propagate to the remote tropics and extra-tropics, modulating weather patterns worldwide[9,10]. The subsequent atmospheric changes may affect the underlying ocean and indirectly influence global climate. For example, the tropical Pacific can modulate remote regional climates through its interactions with the Indian Ocean[11] or the North Pacific[12]. Similarly, the North Atlantic is shown to affect Pacific/North America climate variability via its impacts on the North Pacific[13].

Since the mid-twentieth century, the TIO has experienced a pronounced warming trend far exceeding its natural variability[4,5,14] as its sea surface temperature (SST) increased by over 1 °C, 50–60% more than in other tropical basins (Fig. 1). The change is especially strong in June–September (Supplementary Fig. 1). The TIO warming has been closely tracking the rise of global mean surface temperature since the 1880s[5,15] (Supplementary Fig. 2). Previous research on the TIO warming has focused largely on its regional effects related to atmospheric changes[8,16,17]. Here, we concentrate on its impacts on the AMOC and thus global climate.

First, we conducted an idealized simulation with an ocean–atmosphere coupled general circulation model (GCM), the Community Earth System Model (CESM), wherein we imposed a nearly uniform surface warming of 1 °C onto the TIO region ('TIO+1C'; Methods). Surprisingly, we found that the AMOC strengthened by 5 Sv ($Sv = 10^6\,m^3\,s^{-1}$), about 30% of its mean strength of 17 Sv, after equilibrating for nearly a century (Fig. 2). We conducted two other sensitivity experiments doubling the initial TIO warming ('TIO+2C') and cooling TIO ('TIO–1C'), and found that the AMOC response scaled almost linearly with the imposed TIO temperature anomaly (Fig. 2). Next, we will analyse the TIO+1C experiment in more detail.

Why does the AMOC strengthen in response to the TIO warming? A warmer Indian ocean enhances precipitation and hence latent heat release, inducing a global-scale Gill-type atmospheric response with pronounced stationary Rossby and Kelvin waves. The latter strengthens the Walker cells in the Pacific and the Atlantic[18] (Supplementary Fig. 3). The Atlantic Walker cell strengthening is further amplified by the Bjerknes feedback between zonal winds and zonal SST gradient as the eastern and central equatorial Atlantic SST cools. The cooling is further amplified by the wind–evaporation–SST feedback associated with cross-equatorial winds[19]. This low tropospheric cooling, together with the upper tropospheric warming also induced by the TIO warming, increases atmospheric vertical stability in the tropical Atlantic, reducing rainfall (Fig. 3a) and generating positive anomalies in surface pressure (Fig. 3b).

The reduced precipitation increases sea surface salinity (SSS), particularly over the tropical South Atlantic (Fig. 3c). In several decades, these salinity anomalies are transported to the subpolar North Atlantic by oceanic meridional circulation (Supplementary Fig. 4) further strengthened by the salt–advection feedback[20]. Eventually, surface waters in the subpolar North Atlantic become saltier and denser (Fig. 3c,d), enhancing oceanic deep convection (Supplementary Fig. 5) and accelerating the AMOC (Fig. 3e). To verify this effect, we conducted another simulation ('TAO+0.5PSU'; Methods) wherein a positive SSS anomaly of 0.5 PSU was imposed over the tropical South Atlantic to mimic the salt increase in TIO+1C, and found that the AMOC indeed strengthened by 3–4 Sv after about one century (Fig. 4; Supplementary Figs. 6, 7). Thus, the tropical salinity mechanism can explain roughly 70% of the AMOC strengthening seen in TIO+1C.

Another mechanism potentially maintaining the stronger AMOC is related to remote atmospheric effects of the TIO warming. The TIO convective heat release induces an extratropical atmospheric teleconnection pattern with quasi-stationary atmospheric planetary wave trains propagating poleward and eastward (Supplementary Fig. 8). The resultant meridional dipole of surface pressure over the North Atlantic implies a strengthening of prevailing surface westerly winds south of Greenland (Fig. 3b), consistent with previous modelling studies[16]. The anomalous surface westerlies over the subpolar North Atlantic enhance turbulent latent and

[1]Scripps Institution of Oceanography, University of California-San Diego, La Jolla, CA, USA. [2]Department of Geology and Geophysics, Yale University, New Haven, CT, USA. [3]LOCEAN/IPSL, Sorbonne University, Paris, France. *e-mail: shineng.hu@gmail.com

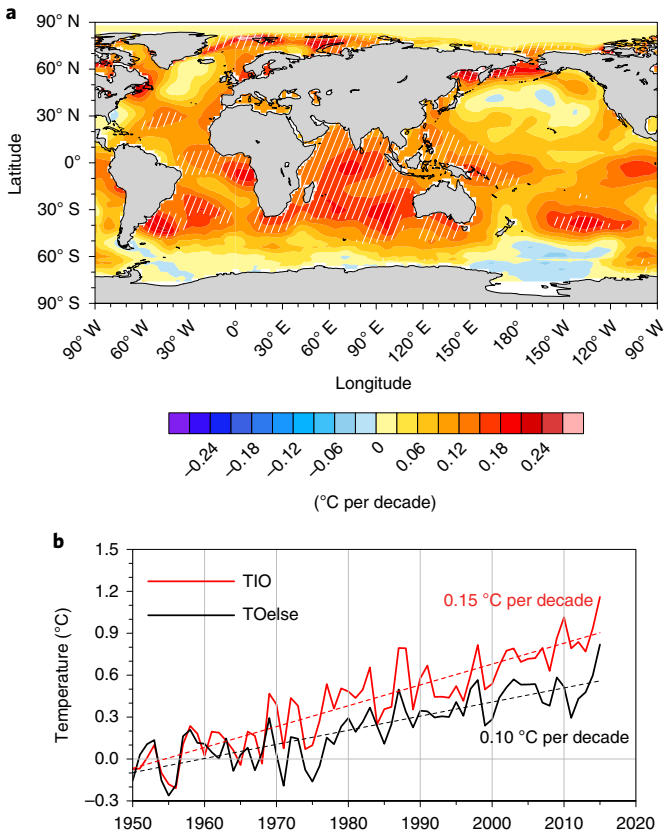

Fig. 1 | TIO warming since the mid-twentieth century. **a**, Long-term trends in annual-mean SST during the period 1950–2015. Hatched areas highlight local long-term trends exceeding 0.5 s.d. per decade, where s.d. is standard deviation of detrended yearly time series. **b**, Annual-mean SST variations for the TIO averaged over the region between 30° S to 30° N and 40° E to 100° E (red) and for the global tropical ocean (30° S to 30° N) but excluding the TIO (TOelse; black). The reference level of the time series has been vertically shifted to have a zero mean during 1950–1959. Linear trends are shown with dashed lines. The ERSST v4 data set is used for analysis.

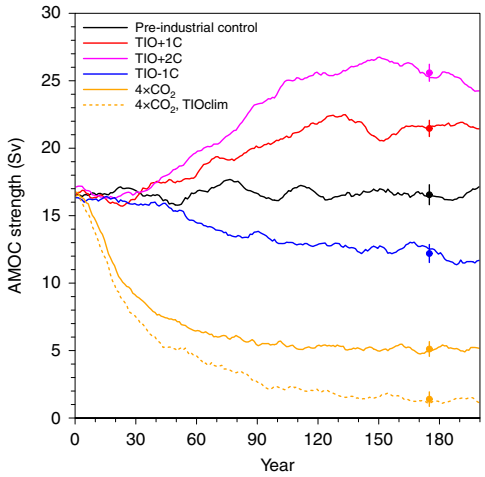

Fig. 2 | The effect of changing TIO SST on the AMOC. The evolution of AMOC intensity in the pre-industrial control and several perturbation experiments: 1 °C TIO warming (TIO+1C), 2 °C TIO warming (TIO+2C), 1 °C TIO cooling (TIO-1C), quadrupling of CO_2 ($4\times CO_2$) and quadrupling of CO_2 but with superimposed climatological TIO SST ($4\times CO_2$, TIOclim). Perturbations are imposed at time zero and maintained for the duration of the experiments. The AMOC intensity is estimated as the maximum streamfunction within 500–5,500 m, 28° N to 90° N. An 11-year running mean is applied to all the curves. The dots and bars indicate average values and interannual variability over the past 50 years, respectively; the latter is estimated as standard deviation relative to an 11-year running mean.

sensible heat fluxes into the atmosphere (Supplementary Fig. 9), which results in surface buoyancy loss favouring a stronger oceanic deep convection and hence a stronger AMOC[21,22]. During the first few decades of integration, this effect appears to be compensated by a rainfall increase (adding buoyancy) but becomes more prominent at the equilibrium stage when the underlying ocean warms significantly (enhancing surface heat fluxes), thus helping to maintain the stronger AMOC (Supplementary Fig. 10).

Even though the imposed TIO warming in TIO+1C is nearly symmetrical about the Equator, the SST response exhibits a strong global interhemispheric asymmetry (Fig. 3a). More heat is transported northward by the accelerated AMOC, resulting in a warmer North Atlantic but a colder South Atlantic. The warming of the North Pacific is associated with the weakening of the Aleutian Low (Fig. 3b) and is partially related to the North Atlantic warming[13]. On a global scale, the anomalous northward ocean heat transport sustains a generally warmer Northern Hemisphere than the Southern Hemisphere, which is balanced by a stronger southward atmospheric heat transport[23] due to the northward shifted intertropical convergence zone (ITCZ) caused by the interhemispheric SST asymmetry (Fig. 3a). Our results imply that a global ITCZ shift does not always require a hemispherically asymmetric forcing in the extratropics as typically suggested[24,25] and could instead originate from the deep tropics.

To further confirm the robustness of the TIO–AMOC link, we conducted similar experiments within a higher-resolution model configuration (Methods) and found a similar climate response (Supplementary Figs. 11–13), although the AMOC response is a little weaker (Fig. 4). Together with the sensitivity simulations that have different magnitudes of the TIO warming (Fig. 2), these results confirm that the TIO warming could strengthen the AMOC, which has broad climate implications.

Climate models generally agree on the slowdown of the AMOC in response to greenhouse warming but disagree on the exact magnitude of the slowdown[2,26–28]. Our results imply a stabilizing effect of the TIO warming on the AMOC intensity under global warming. To confirm this effect, we conducted two additional coupled simulations wherein we abruptly quadrupled the concentration of CO_2, but in the second simulation we suppressed the TIO warming (Methods). In the ordinary CO_2 quadrupling experiment ('$4\times CO_2$'), an active AMOC persists, albeit substantially weaker than in the control state (6 Sv versus 17 Sv; Fig. 2). By contrast, when the TIO warming is suppressed ('$4\times CO_2$, TIOclim'), the AMOC nearly collapses in about a century with only 1–2 Sv remaining, creating an enhanced 'warming hole' over the subpolar North Atlantic (Supplementary Fig. 14). The increase of salinity over the tropical and North Atlantic and enhanced surface westerlies over the subpolar North Atlantic imply the same mechanisms as discussed above, while details are expected to differ under a warming background state (Supplementary Fig. 15; cf. Fig. 3). We repeated this experiment but for an abrupt CO_2 doubling with similar conclusions (Fig. 4).

These global warming experiments confirm that the TIO–AMOC link still holds when the background climate gets warmer and the mean AMOC weakens. Such stabilizing effect of the TIO warming on AMOC slowdown adds another previously overlooked factor in determining the AMOC response to greenhouse warming. Therefore, large uncertainties in the future TIO warming in climate models[4,6] need to be reduced to constrain the future AMOC response.

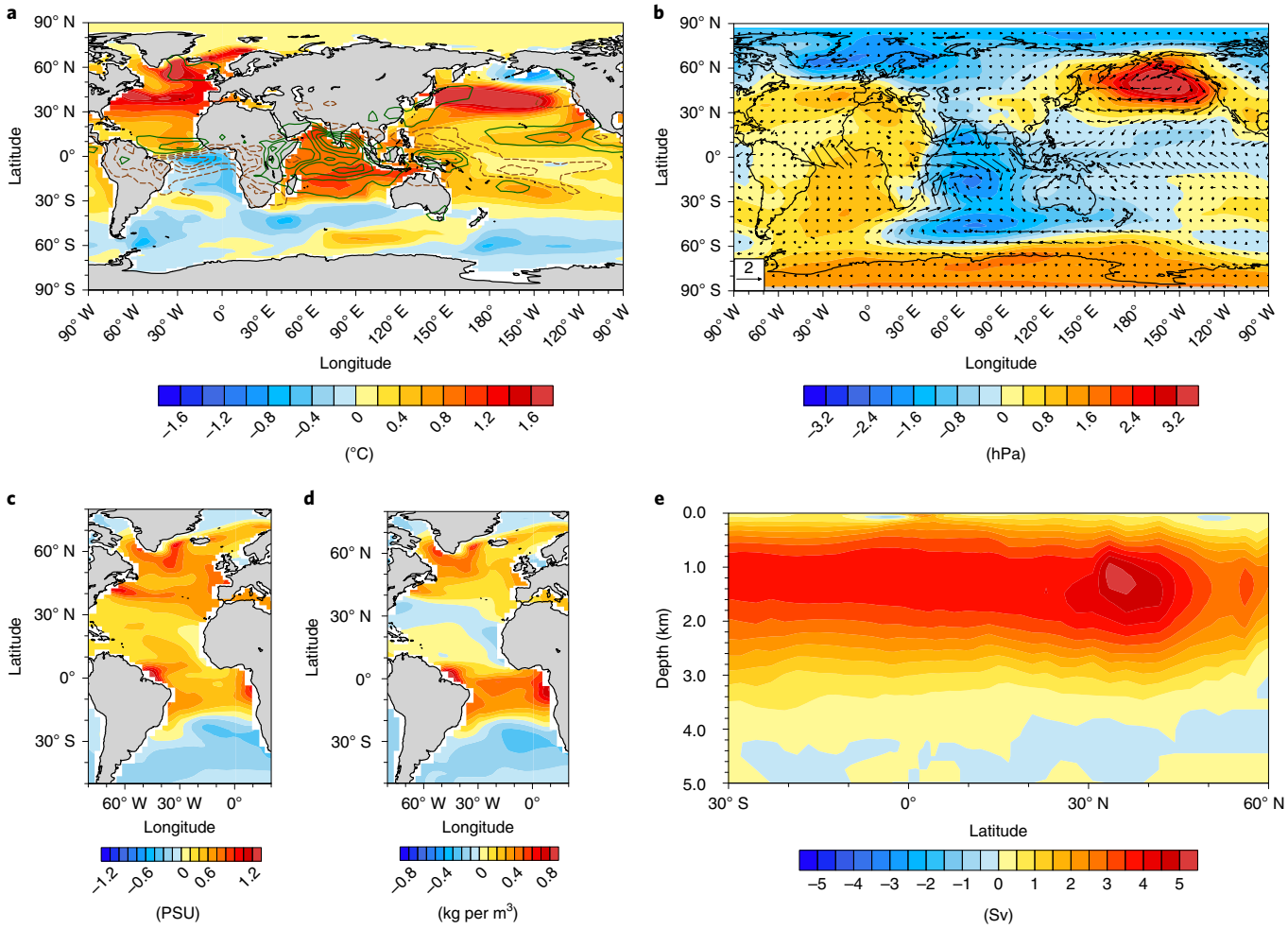

Fig. 3 | Global climate response to TIO warming. a Anomalies in SST (°C) and precipitation (contours; 0.6 mm per day interval; the green and brown contours represent positive and negative precipitation anomalies, respectively, and start from the values of 0.3 mm per day and −0.3 mm per day, respectively). **b**, Anomalies in sea level pressure (hPa) and surface wind (m s^{-1}; arrows). **c**, Anomalies in sea surface salinity (SSS; PSU). **d**, Anomalies in sea surface density (SSD; kg m^{-3}). **e**, Anomalies in AMOC streamfunction, due to the imposed TIO warming of 1 °C. The anomalies are computed for the last 50 years of the TIO+1C experiment with respect to the pre-industrial simulation (Methods).

Given that TIO has been continuously warming since the 1950s or even earlier, has it been already moderating the AMOC response to global warming? Is this moderating effect partially compensated by the concurrent warming in the other two tropical basins? We designed a coupled simulation ('TO+OBS') wherein the observed warming is added in all tropical basins while the interannual variability of tropical SSTs, particularly over the tropical Pacific and Atlantic, is still maintained (Methods). The resultant tropical SST anomalies correspond to about 66 years of the observed trend during 1950–2015 and have an averaged TIO warming of about 1 °C (Supplementary Fig. 16), allowing us to make a direct comparison with the TIO+1C case. In another sensitivity experiment with the observed warming pattern added only to the TIO ('TIO+OBS'; Methods), we found a comparable AMOC response as in the TIO+1C case (Fig. 4; Supplementary Fig. 16), which is expected given similar warming magnitudes averaged over the TIO. Therefore, next we will compare only the TO+OBS and TIO+1C experiments.

In response to the imposed tropical ocean warming, the AMOC strengthens by 2.2 Sv, about half of that in TIO+1C with the imposed warming only over the TIO (Supplementary Fig. 16). The weaker response in the new experiment is explained by the weaker relative TIO warming with respect to the mean surface warming of all tropical oceans (Methods). In TIO+1C, the tropical Pacific also becomes warmer (Fig. 3a), and the achieved TIO warming relative to the mean SST change across all tropical oceans is about 0.5 °C (Fig. 4). But in TO+OBS, the relative TIO warming is smaller, at about 0.3 °C (Fig. 4). Furthermore, we find that across our many experiments it is the relative TIO warming with respect to the mean warming of all tropical oceans that controls the AMOC strength (Fig. 4). In other words, if all tropical oceans warmed uniformly, there would be little or no effect on the AMOC.

The induced positive surface salinity anomalies over the tropical and North Atlantic and westerly wind anomalies over the subpolar North Atlantic, also seen in the TIO+1C case, confirm the central role of the TIO warming in accelerating the AMOC (Supplementary Fig. 16). Note that the simulated SSS changes closely resemble the observed trends since the 1950s, including the fresher Indo-Western Pacific, the saltier Atlantic, the fresher North Pacific and the fresher Southern Ocean[29].

Tentative evidence suggests that the AMOC might have already been slowing over the recent decades[3,27,30]. Recent observational estimates indicate that since the mid-20th century the AMOC has weakened by 3 ± 1 Sv (ref. [31]), on the same order of magnitude as the compensating effects of the TIO warming on the AMOC we found (that is the 2.2 Sv AMOC strengthening generated in the TO+OBS case).

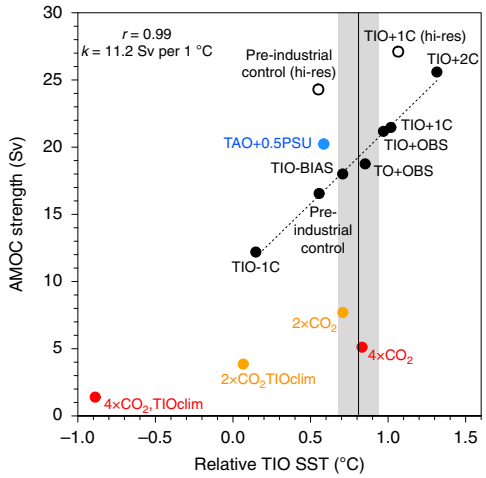

Fig. 4 | TIO control of the AMOC. AMOC strength in different simulations versus relative TIO SST (defined as mean TIO SST relative to the mean SST of all tropical oceans within 30° S to 30° N; Methods). For example, the model climatological relative TIO SST for the pre-industrial state is about 0.55 °C. The vertical line and grey shading indicate the mean value and long-term change of the relative TIO SST, respectively, estimated from ERSST v4 data set for 1950–2015. The change corresponds to the linear trend over 66 years. Each filled circle represents data from one experiment (with the corresponding name) averaged within the last 50 years of the 200-year-long integration. Filled black circles, from the main perturbation experiments of this study, show a tight linear fit ($r = 0.99$) with a regression coefficient of 11.2 Sv per 1 °C of TIO anomaly. The general relation between the AMOC and the relative TIO SST also holds in $2\times CO_2$ and $4\times CO_2$ experiments with suppressed TIO warming (orange and red circles) and in higher-resolution experiments (open circles). Note that the tight TIO–AMOC relationship holds within each group of experiments but not necessarily across different groups as other factors affect the AMOC as well. The blue filled circle indicates an experiment with a superimposed surface salinity anomaly in the tropical Atlantic Ocean (TAO).

In other words, the stabilizing effect of the TIO warming on the AMOC slowdown, together with the potential impacts of anthropogenic aerosols[32,33], may have made the AMOC weakening less pronounced. An accurate quantitative attribution of these effects will require further analysis.

Our results have potential implications for reducing common GCM biases, including a colder than observed Northern Hemisphere[34] (Supplementary Fig. 17), which in some cases can be due to a too weak AMOC simulated by GCMs[35]. Why do some models produce an AMOC weaker than the observed? The persistent cold bias in TIO seen in GCMs can provide a partial explanation. In another sensitivity experiment we imposed a TIO warm anomaly that would be sufficient to correct the multi-model cold bias over the Indian Ocean (Methods). We find that the AMOC strengthens by about 1.5 Sv and the resultant SST warming reduces cold bias at mid and high latitudes in the Atlantic and the Pacific (Supplementary Fig. 17). This suggests that a part of the global SST bias in GCMs can be traced to the Indian Ocean SST bias. In contrast, correcting, for example, the tropical Pacific cold bias without improving the Indian Ocean might weaken the AMOC in those models.

Figure 4 summarizes all the experiments conducted in this study. An extremely tight positive correlation is found between the relative TIO warming and the AMOC strength ($r = 0.99$) for the simulations with imposed tropical temperature anomalies (filled black circles), which also seems to hold for higher-resolution experiments with a stronger AMOC and for CO_2 doubling and quadrupling simulations with suppressed TIO warming (Methods). Thus, our study highlights the important role that the Indian Ocean plays in the global climate system and raises the need for future research of the previously overlooked TIO–AMOC link as part of global teleconnections. Monitoring and simulating correctly the state of TIO is therefore critical for understanding not only regional climate variations in Asia and Africa but also global climate change of the past and future.

Online content

Any methods, additional references, Nature Research reporting summaries, source data, statements of code and data availability and associated accession codes are available at https://doi.org/10.1038/s41558-019-0566-x.

Received: 26 January 2019; Accepted: 29 July 2019;
Published online: 16 September 2019

References

1. Gregory, J. M. et al. A model intercomparison of changes in the atlantic thermohaline circulation in response to increasing atmospheric CO_2 concentration. *Geophys. Res. Lett.* **32**, L12703 (2005).
2. Cheng, W., Chiang, J. C. & Zhang, D. Atlantic meridional overturning circulation (AMOC) in CMIP5 models: RCP and historical simulations. *J. Clim.* **26**, 7187–7197 (2013).
3. Rahmstorf, S. et al. Exceptional twentieth-century slowdown in Atlantic Ocean overturning circulation. *Nat. Clim. Change* **5**, 475–480 (2015).
4. Du, Y. & Xie, S. P. Role of atmospheric adjustments in the tropical Indian Ocean warming during the 20th century in climate models. *Geophys. Res. Lett.* **35,**, L08712 (2008).
5. Roxy, M. K., Ritika, K., Terray, P. & Masson, S. The curious case of Indian Ocean warming. *J. Clim.* **27**, 8501–8509 (2014).
6. Dong, L. & Zhou, T. The Indian Ocean sea surface temperature warming simulated by CMIP5 models during the twentieth century: Competing forcing roles of GHGs and anthropogenic aerosols. *J. Clim.* **27**, 3348–3362 (2014).
7. Sutton, R. T. & Hodson, D. L. Atlantic Ocean forcing of North American and European summer climate. *Science* **309**, 115–118 (2005).
8. Han, W. et al. Indian Ocean decadal variability: a review. *Bull. Am. Meteorol. Soc.* **95**, 1679–1703 (2014).
9. Trenberth, K. E. et al. Progress during TOGA in understanding and modeling global teleconnections associated with tropical sea surface temperatures. *J. Geophys. Res. Oceans* **103**, 14291–14324 (1998).
10. Chiang, J. C. & Sobel, A. H. Tropical tropospheric temperature variations caused by ENSO and their influence on the remote tropical climate. *J. Clim.* **15**, 2616–2631 (2002).
11. Xie, S. P. et al. Indian Ocean capacitor effect on Indo–Western Pacific climate during the summer following El Niño. *J. Clim.* **22**, 730–747 (2009).
12. Di Lorenzo, E. et al. Central Pacific El Niño and decadal climate change in the North Pacific Ocean. *Nat. Geosci.* **3**, 762–765 (2010).
13. Zhang, R. & Delworth, T. L. Impact of the Atlantic multidecadal oscillation on North Pacific climate variability. *Geophys. Res. Lett.* **34**, L23708 (2007).
14. Lee, S. K. et al. Pacific origin of the abrupt increase in Indian Ocean heat content during the warming hiatus. *Nat. Geosci.* **8**, 445–449 (2015).
15. Abish, B., Cherchi, A. & Ratna, S. B. ENSO and the recent warming of the Indian Ocean. *Int. J. Climatol.* **38**, 203–214 (2018).
16. Hoerling, M. P., Hurrell, J. W. & Xu, T. Tropical origins for recent North Atlantic climate change. *Science* **292**, 90–92 (2001).
17. Cherchi, A. et al. The influence of tropical Indian Ocean SST on the Indian summer monsoon. *J. Clim.* **20**, 3083–3105 (2007).
18. Cai, W. et al. Pantropical climate interactions. *Science* **363**, eaav4236 (2019).
19. Xie, S. P. & Philander, S. G. H. A coupled ocean–atmosphere model of relevance to the ITCZ in the eastern Pacific. *Tellus A Dyn. Meteorol. Oceanogr.* **46**, 340–350 (1994).
20. Stommel, H. Thermohaline convection with two stable regimes of flow. *Tellus* **13**, 224–230 (1961).
21. Eden, C. & Jung, T. North Atlantic interdecadal variability: Oceanic response to the North Atlantic oscillation (1865–1997). *J. Clim.* **14**, 676–691 (2001).
22. Delworth, T. L. et al. The North Atlantic oscillation as a driver of rapid climate change in the Northern Hemisphere. *Nat. Geosci.* **9**, 509–512 (2016).
23. Frierson, D. M. et al. Contribution of ocean overturning circulation to tropical rainfall peak in the Northern Hemisphere. *Nat. Geosci.* **6**, 940–944 (2013).
24. Kang, S. M., Held, I. M., Frierson, D. M. & Zhao, M. The response of the ITCZ to extratropical thermal forcing: Idealized slab-ocean experiments with a GCM. *J. Clim.* **21**, 3521–3532 (2008).

25. Schneider, T., Bischoff, T. & Haug, G. H. Migrations and dynamics of the intertropical convergence zone. *Nature* **513**, 45–53 (2014).
26. Bakker, P. et al. Fate of the Atlantic meridional overturning circulation: strong decline under continued warming and Greenland melting. *Geophys. Res. Lett.* **43**, 12252–12260 (2016).
27. Sévellec, F., Fedorov, A. V. & Liu, W. Arctic sea-ice decline weakens the Atlantic meridional overturning circulation. *Nat. Clim. Change* **7**, 604–610 (2017).
28. Liu, W., Xie, S. P., Liu, Z. & Zhu, J. Overlooked possibility of a collapsed Atlantic meridional overturning circulation in warming climate. *Sci. Adv.* **3**, e1601666 (2017).
29. Durack, P. J. & Wijffels, S. E. Fifty-year trends in global ocean salinities and their relationship to broad-scale warming. *J. Clim.* **23**, 4342–4362 (2010).
30. Smeed, D. A. et al. The North Atlantic Ocean is in a state of reduced overturning. *Geophys. Res. Lett.* **45**, 1527–1533 (2018).
31. Caesar, L., Rahmstorf, S., Robinson, A., Feulner, G. & Saba, V. Observed fingerprint of a weakening Atlantic Ocean overturning circulation. *Nature* **556**, 191 (2018).
32. Delworth, T. L. & Dixon, K. W. Have anthropogenic aerosols delayed a greenhouse gas-induced weakening of the North Atlantic thermohaline circulation? *Geophys. Res. Lett.* **33**, L02606 (2006).
33. Shi, J. R., Xie, S. P. & Talley, L. D. Evolving relative importance of the Southern Ocean and North Atlantic in anthropogenic ocean heat uptake. *J. Clim.* **31**, 7459–7479 (2018).
34. Burls, N. J., Muir, L., Vincent, E. M. & Fedorov, A. Extra-tropical origin of equatorial Pacific cold bias in climate models with links to cloud albedo. *Clim. Dyn.* **49**, 2093–2113 (2017).
35. Wang, C., Zhang, L., Lee, S. K., Wu, L. & Mechoso, C. R. A global perspective on CMIP5 climate model biases. *Nat. Clim. Change* **4**, 201–205 (2014).

Acknowledgements

A.V.F. was supported by grants from NSF (OCE-1756682, OPP-1741847), the ARCHANGE project of the "Make our planet great again" programme (CNRS, France) and the Guggenheim fellowship. S.H. was supported by the Scripps Institutional Postdoctoral Fellowship Program. We also acknowledge computational support from the NSF/NCAR Yellowstone/Cheyenne Supercomputing Center.

Author contributions

S.H. conceived the study, conducted the numerical simulations, performed the data analysis and led the writing of the manuscript. S.H. and A.V.F. together interpreted and explained the results and edited the manuscript.

Competing interests

The authors declare no competing interests.

Additional information

Supplementary information is available for this paper at https://doi.org/10.1038/s41558-019-0566-x.

Reprints and permissions information is available at www.nature.com/reprints.

Correspondence and requests for materials should be addressed to S.H.

Peer review information: *Nature Climate Change* thanks Claudia Frauen, Changhyun Yoo and the other, anonymous, reviewer(s) for their contribution to the peer review of this work.

Publisher's note: Springer Nature remains neutral with regard to jurisdictional claims in published maps and institutional affiliations.

Methods

Observational data sets. For SST, we use National Oceanic and Atmospheric Administration (NOAA) Extended Reconstructed Sea Surface Temperature (ERSST) v4 provided by NOAA Earth System Research Laboratory (ESRL) Physical Sciences Division (http://www.esrl.noaa.gov/psd/data). For global surface temperatures, we use Goddard Institute for Space Studies (GISS) Surface Temperature Analysis (GISTEMP) with a 1,200 km smoothing[36]. Anomalies are computed with respect to the 30-year climatology during 1951–1980.

General circulation model. In this study, we use a climate GCM developed by the National Center for Atmospheric Research (NCAR), CESM[37] version 1.0.6 with a T31_g37 resolution (corresponding to roughly 4° for the atmosphere, and 4° of longitude and 2° of latitude for the ocean, with latitudinal resolution increasing to 0.5° near the Equator and in high latitudes). In addition, we have conducted sensitivity tests using a higher-resolution CESM configuration f19_g16 (with a horizontal resolution of about 2° for the atmosphere and 1° of longitude and 0.5° of latitude for the ocean), and the results were generally similar. It is important that the two model configurations have different mean AMOC strengths: 17 and 24 Sv, respectively. This can be compared to about 18 Sv estimated from ocean reanalysis data sets for 1960–2007[38] and 17 Sv at 26.5° N from the Rapid Climate Change programme (RAPID) observations for 2004–2017[28].

Coupled climate simulations. Here we summarize the main simulations conducted in this study. All the simulations are integrated for 200 years, and the past 50 years are averaged to obtain a quasi-equilibrated climate mean state, unless mentioned differently. The pre-industrial control case is used as the reference simulation. In 'TIO+1C', we restore the tropical Indian Ocean SST to a seasonally varying climatology warmer than in the pre-industrial control run by about 1 °C. Similarly, sensitivity simulations 'TIO+2C' and 'TIO−1C' imply a TIO warming of 2 °C and cooling of 1 °C, respectively. These four experiments demonstrate that the TIO warming strengthens the AMOC and that the AMOC response scales almost linearly with the imposed TIO temperature anomaly.

In '4×CO_2', we abruptly increase CO_2 concentration by a factor of 4. In '4×CO_2, TIOclim', we abruptly quadruple the CO_2 level but maintain the pre-industrial SST climatology in the tropical Indian Ocean. Similarly, we conducted another two simulations, '2×CO_2' and '2×CO_2, TIOclim', but for an abrupt doubling of CO_2. In 'TIO-BIAS', we impose a warm-temperature anomaly in the tropical Indian Ocean that would compensate the multi-model mean cold SST bias found in 34 CMIP5 models. In all such simulations wherein we impose temperature anomalies, we restore SST in the tropical Indian Ocean (30° S to 30° N, 40° E to 100° E, with a 5° outer buffering zone) to a target temperature with a relaxation timescale of 10 days. In 'TAO+0.5PSU', we impose a positive salinity anomaly (~0.5 PSU) in the tropical Atlantic Ocean (25° S to 5° N, with a 5° outer buffering zone) using a similar restoring technique but for salinity.

To further test our conclusions, we conduct two sensitivity simulations by repeating the pre-industrial control run and TIO+1C within a higher-resolution model configuration (f19_g16).

Finally, we explore the potential effects of the observed ocean warming since the 1950s across the entire tropics by conducting two coupled simulations. First, we restore tropical SST within 30° S to 30° N (again, with a 5° outer buffering zone) towards a seasonally varying target temperature that is equal to the pre-industrial control climatology plus the observed warming anomaly whose magnitude is equivalent to 66 years of the long-term trend during 1950–2015. The simulation is integrated for 100 years, and then we estimate the averaged restoring heat flux for each month over the past 80 years. Next, we apply this seasonally varying heat flux to another coupled simulation ('TO+OBS'). The resultant climate has a warmer tropical SST than the pre-industrial control climate and closely resembles the observations of the past decades. The main advantage of imposing the observed SST anomalies through heat fluxes, rather than through restoring as done at the first step, is that the interannual variability of tropical SSTs, particularly in the tropical Pacific and Atlantic, is not damped. This is not a big concern when we restore temperature in the Indian Ocean because the TIO interannual variability is relatively small compared with that in the other two tropical ocean basins and is almost an order of magnitude smaller than the observed TIO warming since the 1950s (Fig. 1).

We applied the same two-step modelling technique and conducted a similar simulation, 'TIO+OBS', but with the observed warming applied only to the tropical Indian Ocean. The AMOC response has a similar magnitude as our main simulation, TIO+1C (Supplementary Fig. 16). This is expected because the TIO warming magnitude is similar in the two cases, 0.91 °C for TIO+OBS and 0.96 °C for TIO+1C, when averaged within 25° S to 25° N, 45° E to 95° E, during the past 50 years of integration.

For Fig. 4, the relative TIO SST is defined as the mean tropical Indian Ocean SST (30° S to 30° N, 40° E to 100° E) minus mean SST for all tropical oceans (30° S to 30° N), following ref. [39].

CMIP5 model bias analysis. We examined SST biases in 34 climate models from the Coupled Model Intercomparison Project Phase 5 (CMIP5) available at https://cmip.llnl.gov/cmip5. We chose the 1900–2005 interval in historical simulations and compared it with the NOAA ERSST v4 data set. The 34 climate models are ACCESS1-0, ACCESS1-3, CanESM2, CCSM4, CMCC-CESM, CMCC-CM, CMCC-CMS, CNRM-CM5, CNRM-CM5-2, CSIRO-Mk3-6-0, GFDL-CM3, GFDL-ESM2G, GFDL-ESM2M, GISS-E2-H, GISS-E2-H-CC, GISS-E2-R, GISS-E2-R-CC, HadCM3, HadGEM2-AO, HadGEM2-ES, inmcm4, IPSL-CM5A-LR, IPSL-CM5A-MR, IPSL-CM5B-LR, MIROC5, MIROC-ESM, MIROC-ESM-CHEM, MPI-ESM-LR, MPI-ESM-MR, MPI-ESM-P, MRI-CGCM3, MRI-ESM1, NorESM1-M, NorESM1-ME.

Data availability

The NOAA ERSST v4 data set is available at http://www.esrl.noaa.gov/psd/data. The data that support the findings of this study are available from the corresponding author upon request.

Code availability

We used the NCAR Command Language (NCL)[40] for all the analyses and figures in this study, which is available from https://doi.org/10.5065/D6WD3XH5.

References

36. Hansen, J., Ruedy, R., Sato, M. & Lo, K. Global surface temperature change. *Rev. Geophys.* **48**, RG4004 (2010).
37. Gent, P. R. et al. The community climate system model version 4. *J. Clim.* **24**, 4973–4991 (2011).
38. Karspeck, A. R. et al. Comparison of the Atlantic meridional overturning circulation between 1960 and 2007 in six ocean reanalysis products. *Clim. Dyn.* **49**, 957–982 (2017).
39. Xie, S. P. et al. Global warming pattern formation: sea surface temperature and rainfall. *J. Clim.* **23**, 966–986 (2010).
40. NCAR Command Language v.6.6.2 (UCAR/NCAR/CISL/TDD, 2019); https://doi.org/10.5065/D6WD3XH5

nature climate change

SUPPLEMENTARY INFORMATION

https://doi.org/10.1038/s41558-019-0566-x

In the format provided by the authors and unedited.

Indian Ocean warming can strengthen the Atlantic meridional overturning circulation

Shineng Hu[1]* and Alexey V. Fedorov[2,3]

[1]Scripps Institution of Oceanography, University of California-San Diego, La Jolla, CA, USA. [2]Department of Geology and Geophysics, Yale University, New Haven, CT, USA. [3]LOCEAN/IPSL, Sorbonne University, Paris, France. *e-mail: shineng.hu@gmail.com

Supplementary information for:

Indian Ocean warming can strengthen the Atlantic meridional overturning circulation

Shineng Hu[1*], Alexey V. Fedorov[2]

[1] Scripps Institution of Oceanography, University of California-San Diego, La Jolla, CA, USA

[2] Department of Geology and Geophysics, Yale University, New Haven, CT, USA

[*]Corresponding author: Shineng Hu (shineng.hu@gmail.com)

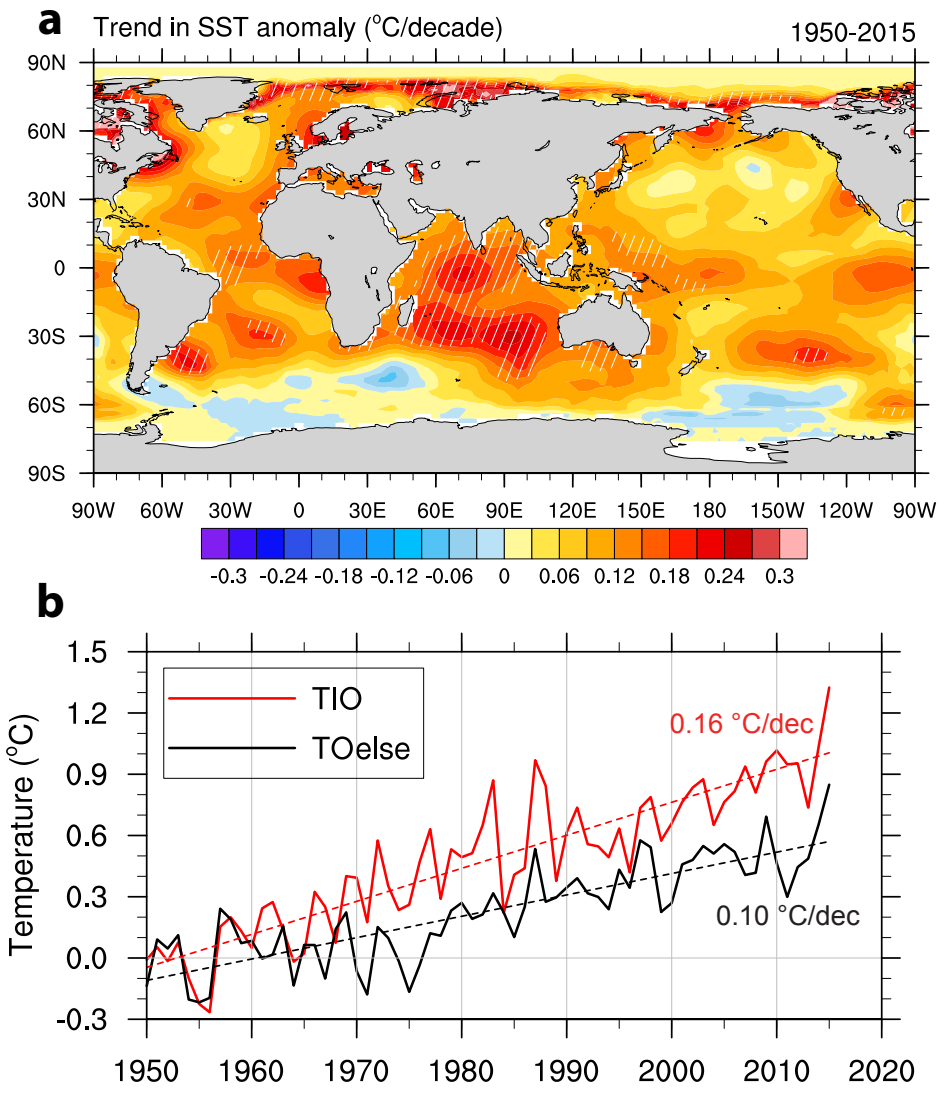

Supplementary Figure 1 | Tropical Indian Ocean warming since the mid 20th century. As in Figure 1, but for boreal summer values. (a) Long-term trends in June-September SST during the period of 1950-2015. Hatched areas highlight local long-term trends exceeding 0.5 std/decade, where std is standard deviation of detrended yearly time series. (b) June-September SST variations for the tropical Indian Ocean (TIO) averaged within the region 30°S-30°N, 40°E-100°E (red) and for the Global Tropical Ocean (30°S-30°N) but excluding the TIO (black). The reference level of the time series has been vertically shifted to have a zero mean during 1950-1959. Linear trends are shown with dashed lines.

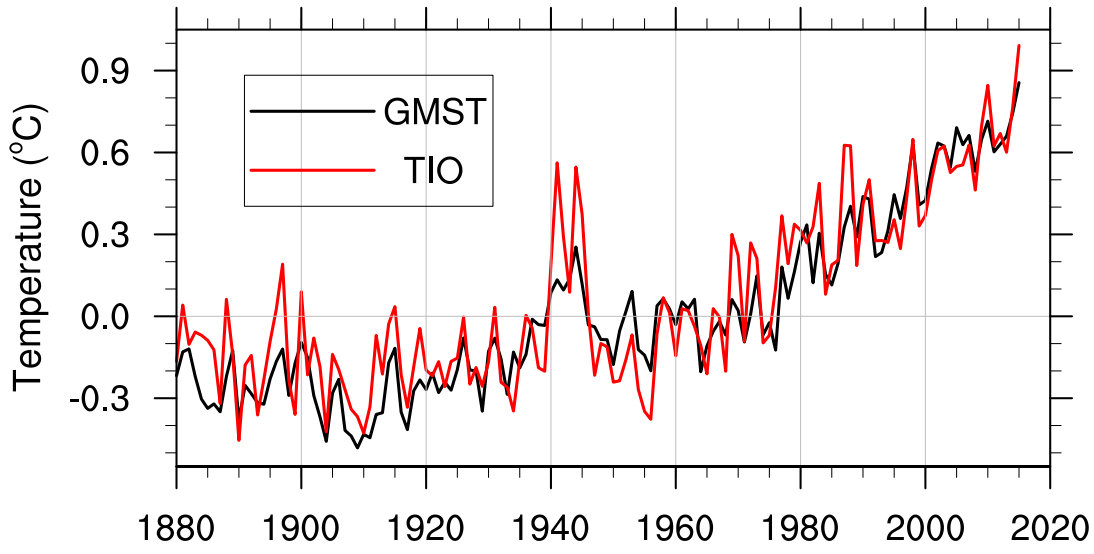

Supplementary Figure 2 | Tropical Indian Ocean warming tracks global warming. A comparison between variations in annual-mean TIO SST averaged within 30°S-30°N, 40°E-100°E and global mean surface temperature (GMST) since 1880. Temperature anomalies are computed with respect to the 30-year climatology during 1951-1980.

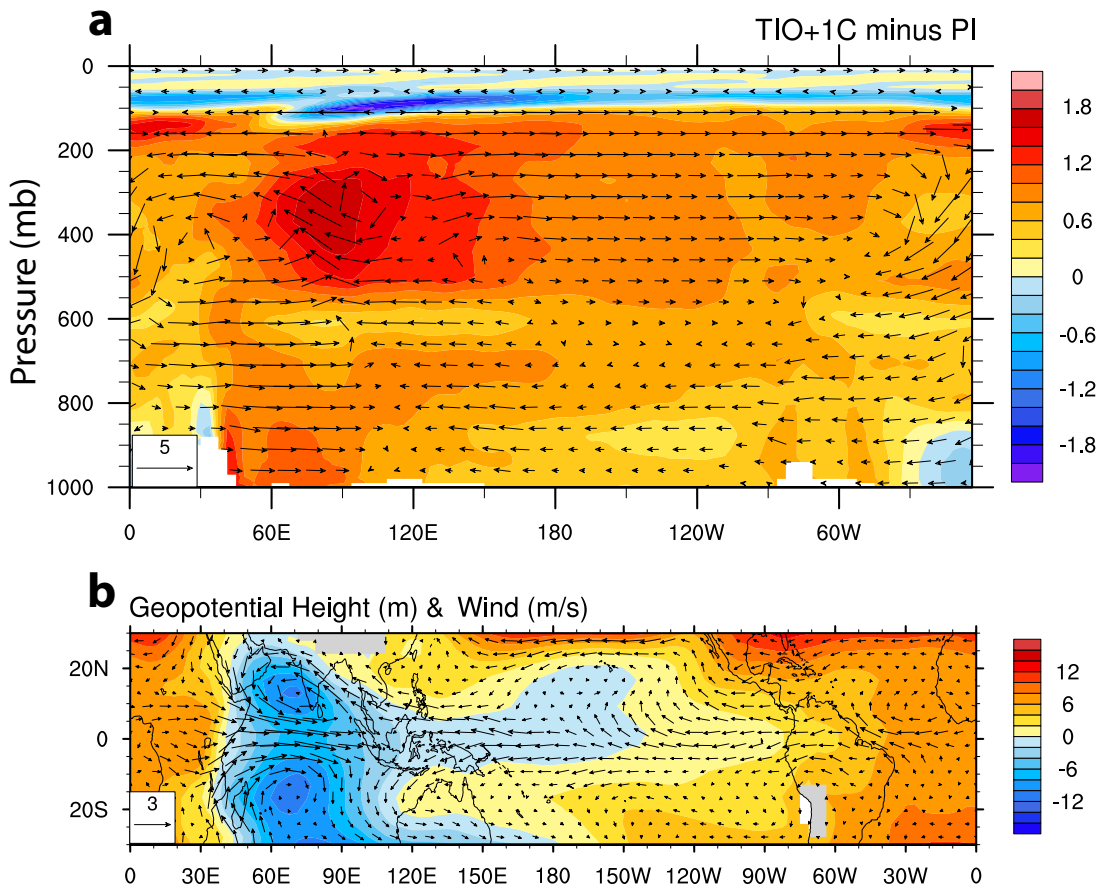

Supplementary Figure 3 | Tropical atmospheric response to Indian Ocean warming. (a) Anomalies in the Walker circulation (vectors) and tropospheric temperature (shadings; °C) averaged within the equatorial band (5°S-5°N). Zonal wind has units of m/s, while vertical velocity has units of 10^{-2} Pa/s. (b) Anomalies in geopotential height (m) and wind (m/s) at 850 hPa. The anomalies are computed for the last 50 years of the TIO+1C experiment with respect to the pre-industrial simulation (Methods). Note the typical Gill-type response to heating in the Indo-Pacific and the strengthening of the Walker cells in the Pacific and Atlantic oceans.

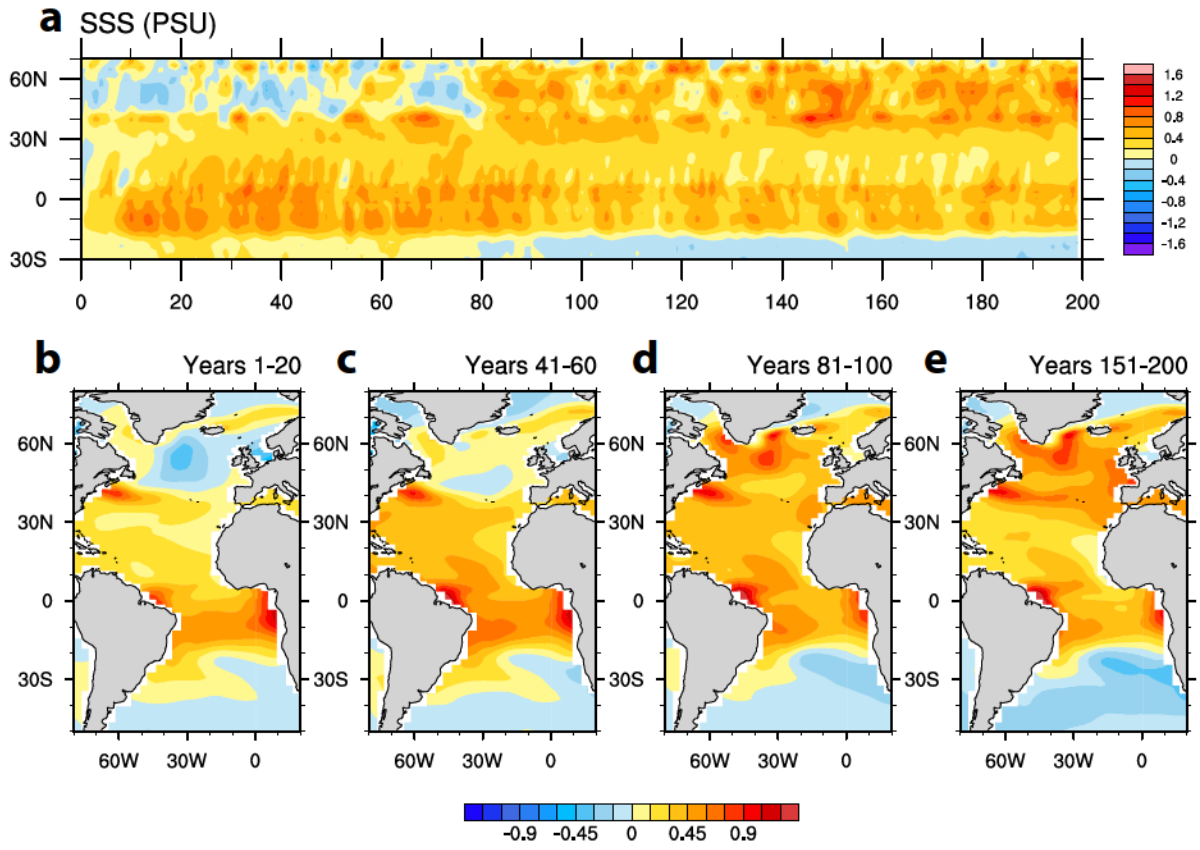

Supplementary Figure 4 | Atlantic salinity response to the tropical Indian Ocean warming. (a) A Hovmoller diagram of annual-mean zonal-mean sea surface salinity (SSS) anomaly averaged within 70ºW-0° in TIO+1C with respect to PI. (b-e) The evolution of SSS anomalies during years 1-20, 41-60, 81-100, and 151-200, respectively.

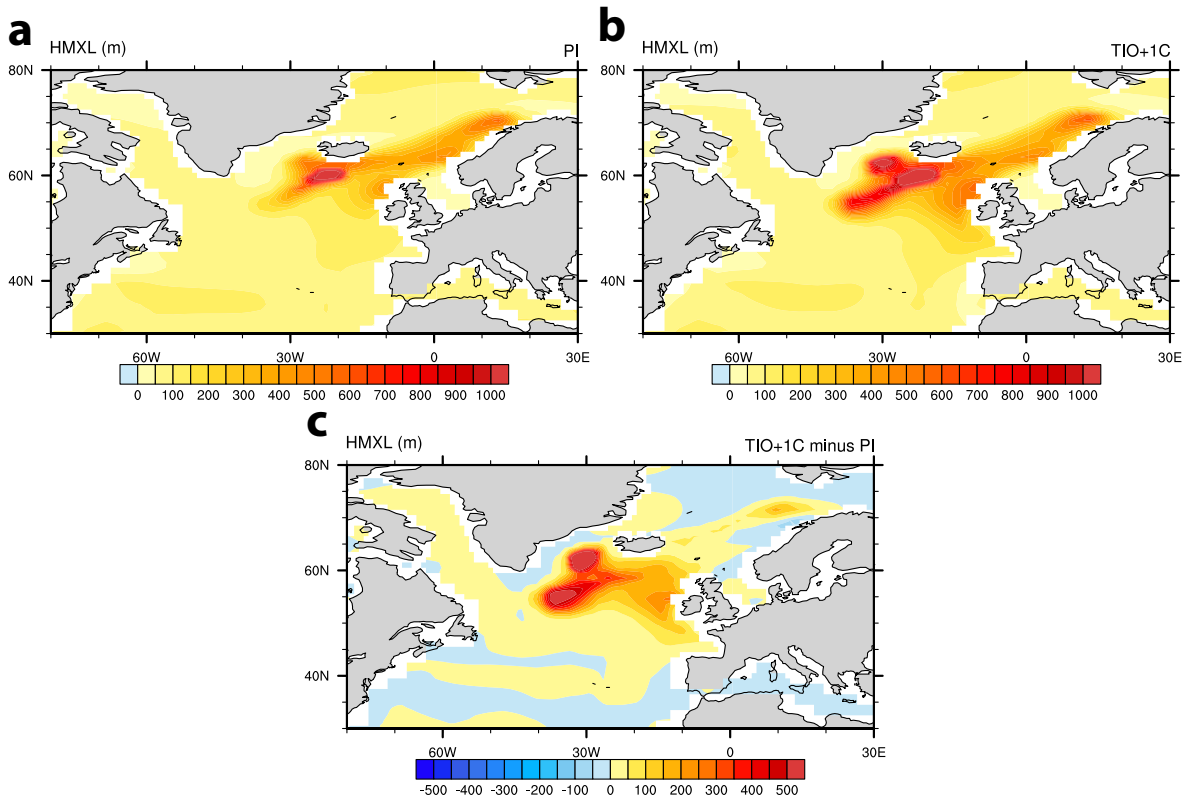

Supplementary Figure 5 | Atlantic mixed layer depth response to the tropical Indian Ocean warming. (a,b) March ocean mixed layer depth (units: m) in two experiments (a) PI and (b) TIO+1C (Methods) averaged within the last 50 years of the integration. (c) March ocean mixed layer depth difference between TIO+1C and PI.

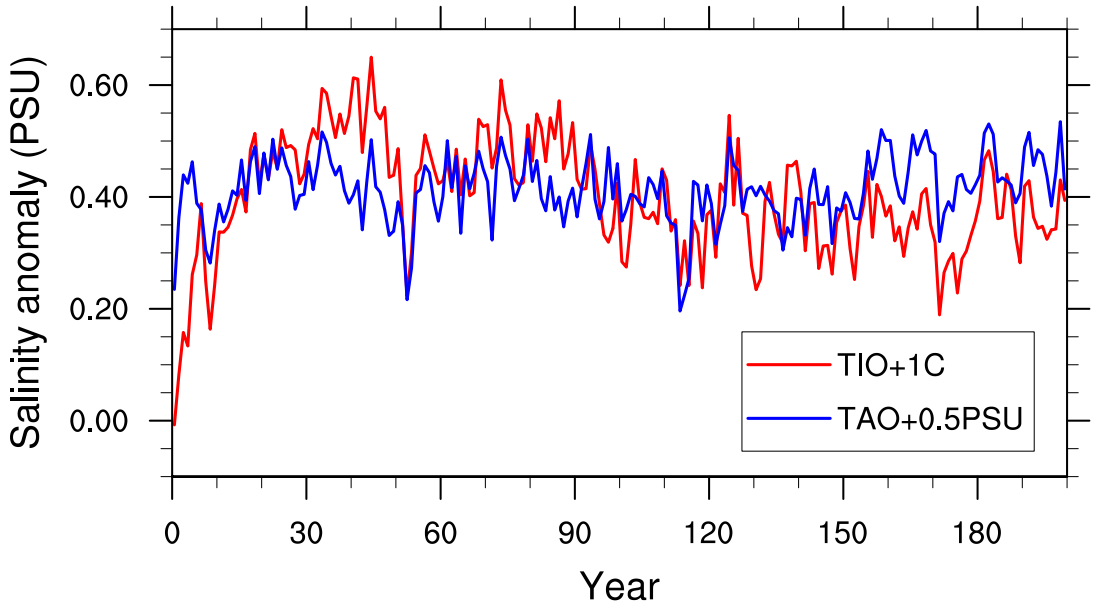

Supplementary Figure 6 | Tropical Atlantic salinity changes in two sensitivity experiments. The evolution of annual-mean sea surface salinity anomalies over the tropical Atlantic (25°S-5°N, 60°W-20°E) for the TIO+1C and TAO+0.5PSU cases, with respect to the pre-industrial simulation. The comparison suggests that the latter run closely mimics the tropical Atlantic salinity changes generated in the former, TIO warming experiment.

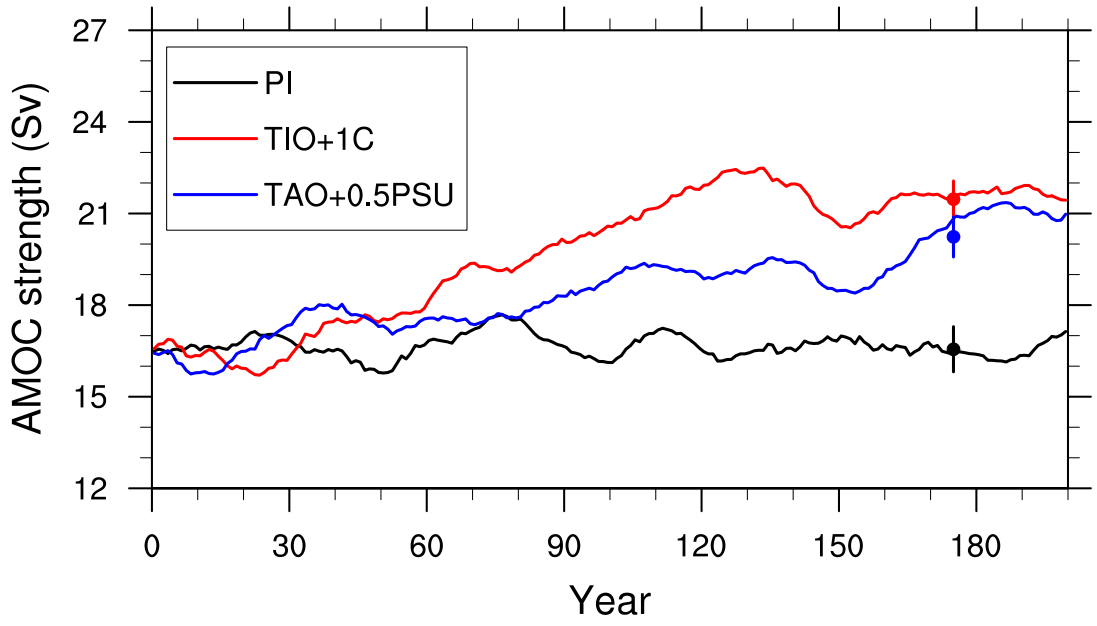

Supplementary Figure 7 | AMOC changes in response to a more saline tropical North Atlantic. The evolution of AMOC intensity for the experiment with a superimposed 0.5 psu salinity anomaly over the tropical South Atlantic Ocean ('TAO+0.5PSU'). See more details in the Methods section. The pre-industrial case ('PI') and the 1°C TIO warming case ('TIO+1C') are shown for comparison. The AMOC intensity is estimated as the maximum streamfunction within 500-5500 m, 28°N-90°N. An 11-year running mean is applied to all the curves. The dots and bars indicate average values and interannual variability over the last fifty years, respectively; the latter is estimated as standard deviation relative to an 11-year running mean.

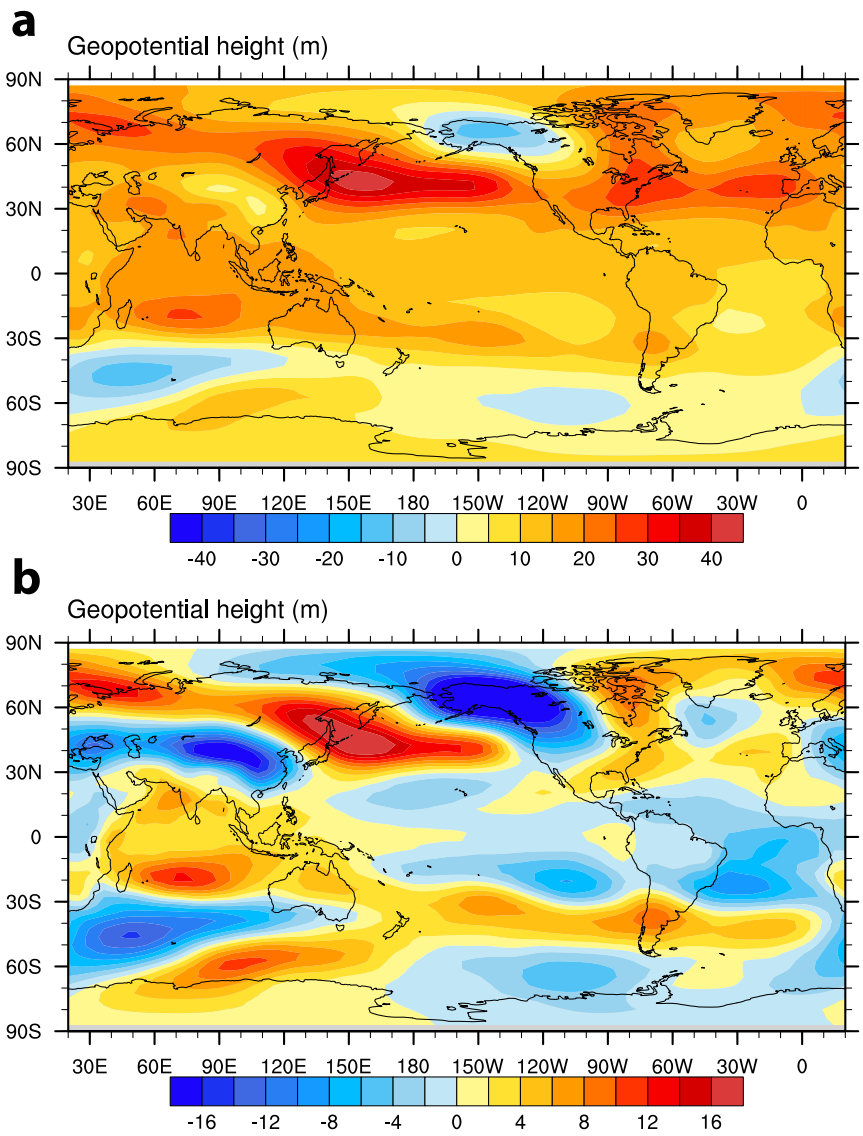

Supplementary Figure 8 | Quasi-stationary atmospheric Rossby wave trains generated by the tropical Indian Ocean warming. (a) Anomalies in geopotential height at the level of 510 in CESM's hybrid vertical coordinate, close to 500 hPa, for the 1°C TIO warming (experiment TIO+1C). (b) As in panel (a) but with the zonal mean removed. Anomalies are averaged within the last 50 years of the integrations. The wave train is much more pronounced in the Northern Hemisphere.

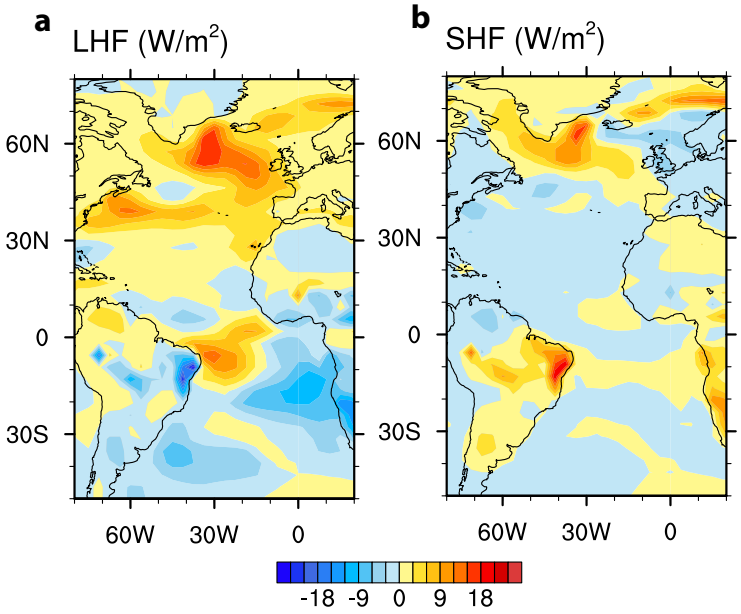

Supplementary Figure 9 | North Atlantic turbulent heat flux response to the tropical Indian Ocean warming. Anomalies in surface (a) latent heat flux (W/m^2) and (b) sensible heat flux (W/m^2), due to the imposed TIO warming of 1ºC. The anomalies are computed for the last 50 years of the TIO+1C experiment with respect to the pre-industrial simulation (Methods).

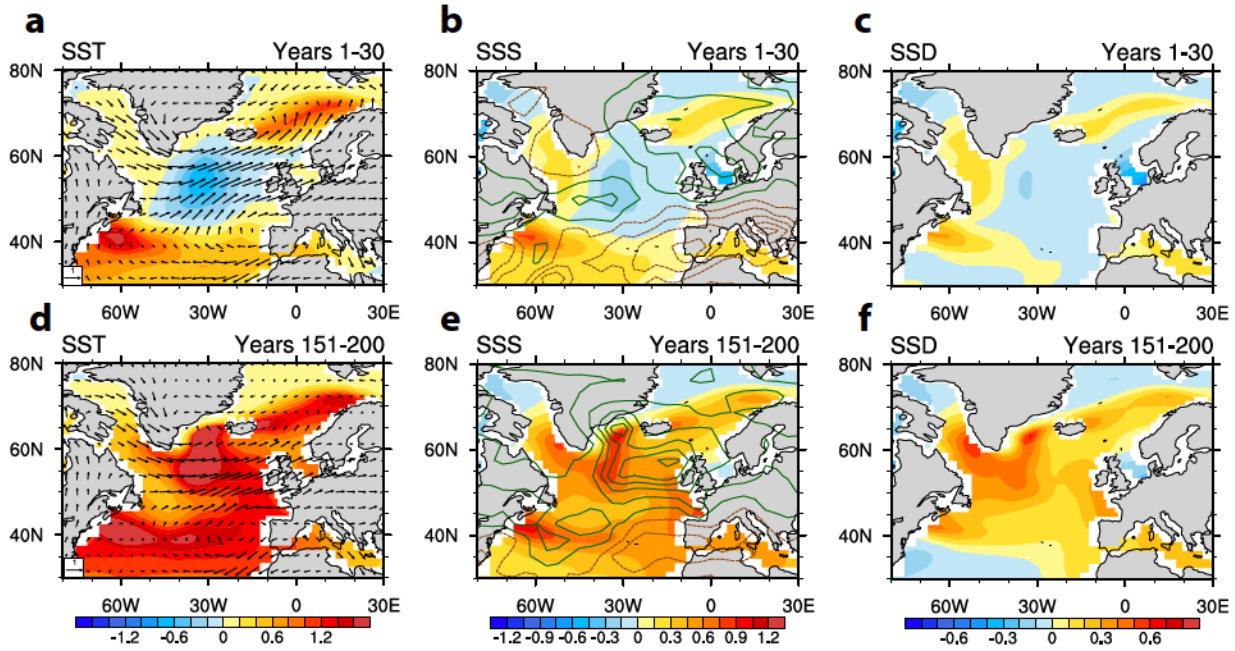

Supplementary Figure 10 | North Atlantic initial and equilibrium climate responses to the tropical Indian Ocean warming. Anomalies in (a,d) SST (°C) and surface winds (m/s), (b,e) SSS (psu) and precipitation (contours; 0.1 mm/day interval) and (c,f) SSD (kg/m3) for the initial (the first 30 years) and equilibrium (the last 50 years) stages of the TIO+1C experiment with respect to the pre-industrial simulation (Methods). In panels b and e, green and brown contours represent positive and negative precipitation anomalies, respectively; the contours start from 0.05 mm/day and -0.05 mm/day.

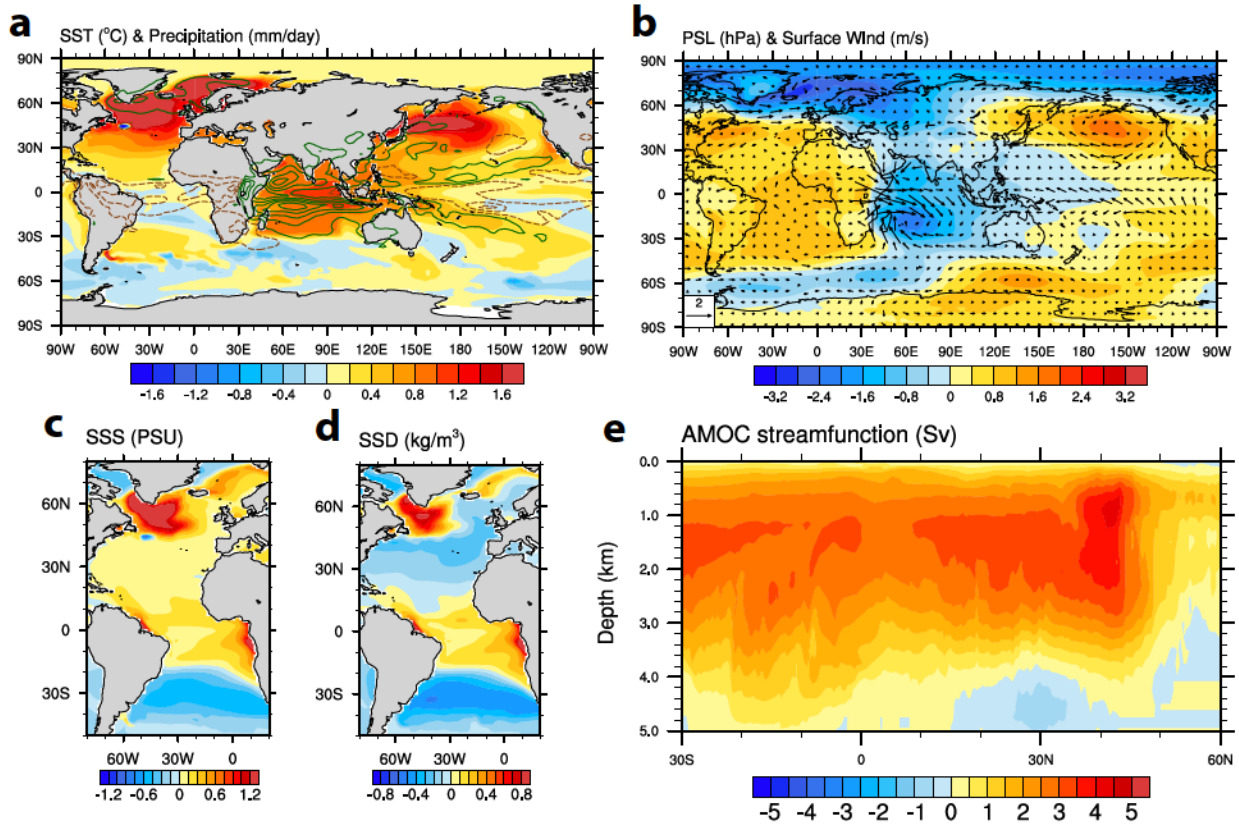

Supplementary Figure 11 | Climate response to the tropical Indian Ocean warming in the higher-resolution simulation. Anomalies in (a) SST and precipitation (contours; 0.6 mm/day interval), (b) sea level pressure and surface wind (arrows), (c) sea surface salinity (psu), and (d) sea surface density (kg/m^3), and in (e) AMOC streamfunction, induced by the imposed TIO warming of 1ºC. The anomalies are computed for the last 50 years of the TIO+1C experiment with respect to the pre-industrial simulation using a higher-resolution configuration of CESM (f19_g16; Methods). In panel (a), the green and brown contours represent positive and negative precipitation anomalies, respectively; the contours start from the values of 0.3 mm/day and -0.3 mm/day. Note the similarities with our main simulations (*c.f.* Fig. 3).

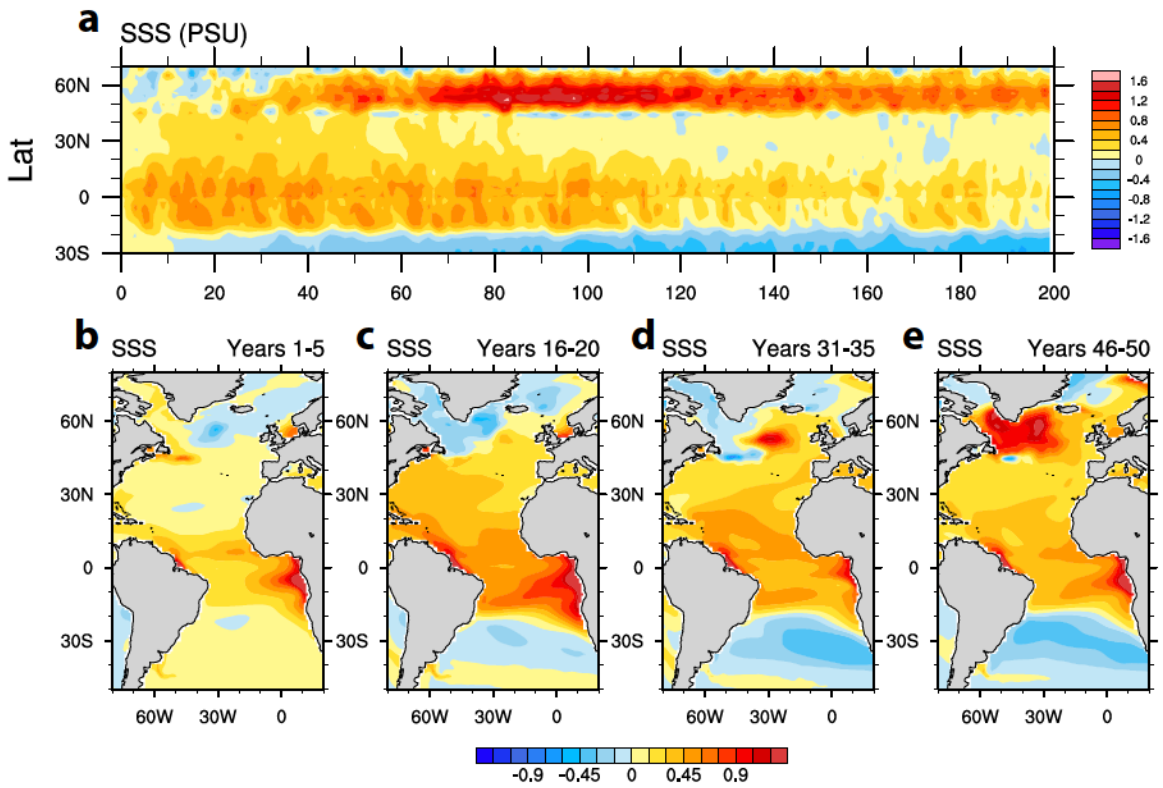

Supplementary Figure 12 | Atlantic salinity response to the tropical Indian Ocean warming in the higher-resolution simulation. (a) A Hovmoller diagram of annual-mean zonal-mean sea surface salinity (SSS) anomaly averaged within 70ºW-0° in TIO+1C with respect to the PI control. (b-e) The evolution of SSS anomalies during years 1-5, 16-20, 31-35, and 46-50, respectively. Note the similarities with our main simulations (*c.f.* Supplementary Fig. 4).

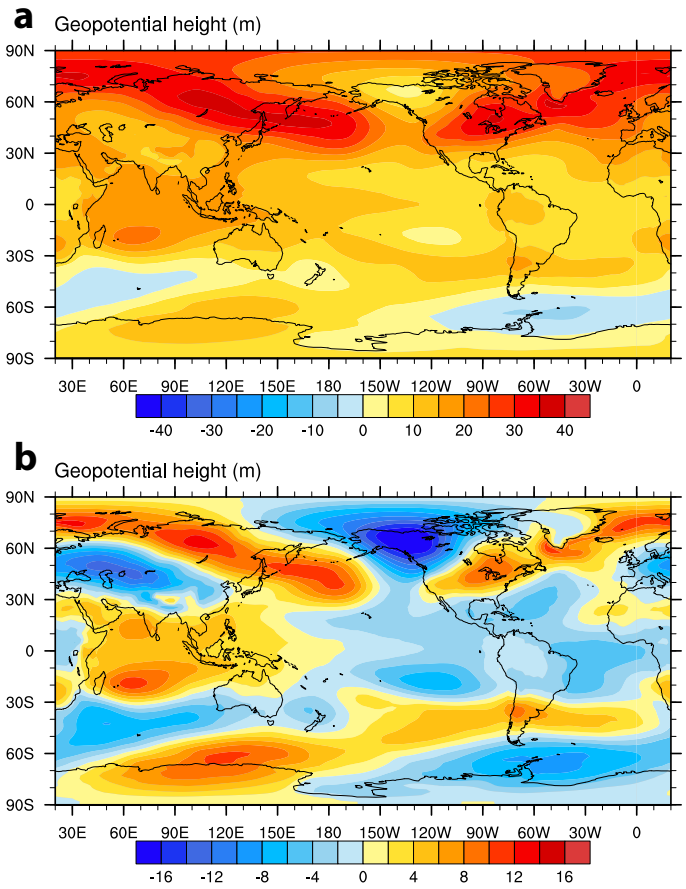

Supplementary Figure 13 | Quasi-stationary atmospheric Rossby wave trains generated by the tropical Indian Ocean warming in the higher-resolution simulation. (a) Anomalies in geopotential height at the level of 510 in CESM's hybrid vertical coordinate, close to 500 hPa, for the 1°C TIO warming (experiment TIO+1C). (b) As in panel a but with the zonal mean removed. Anomalies are averaged within the last 50 years of integration. Note the similarities with our main simulations (*c.f.* Supplementary Fig. 8).

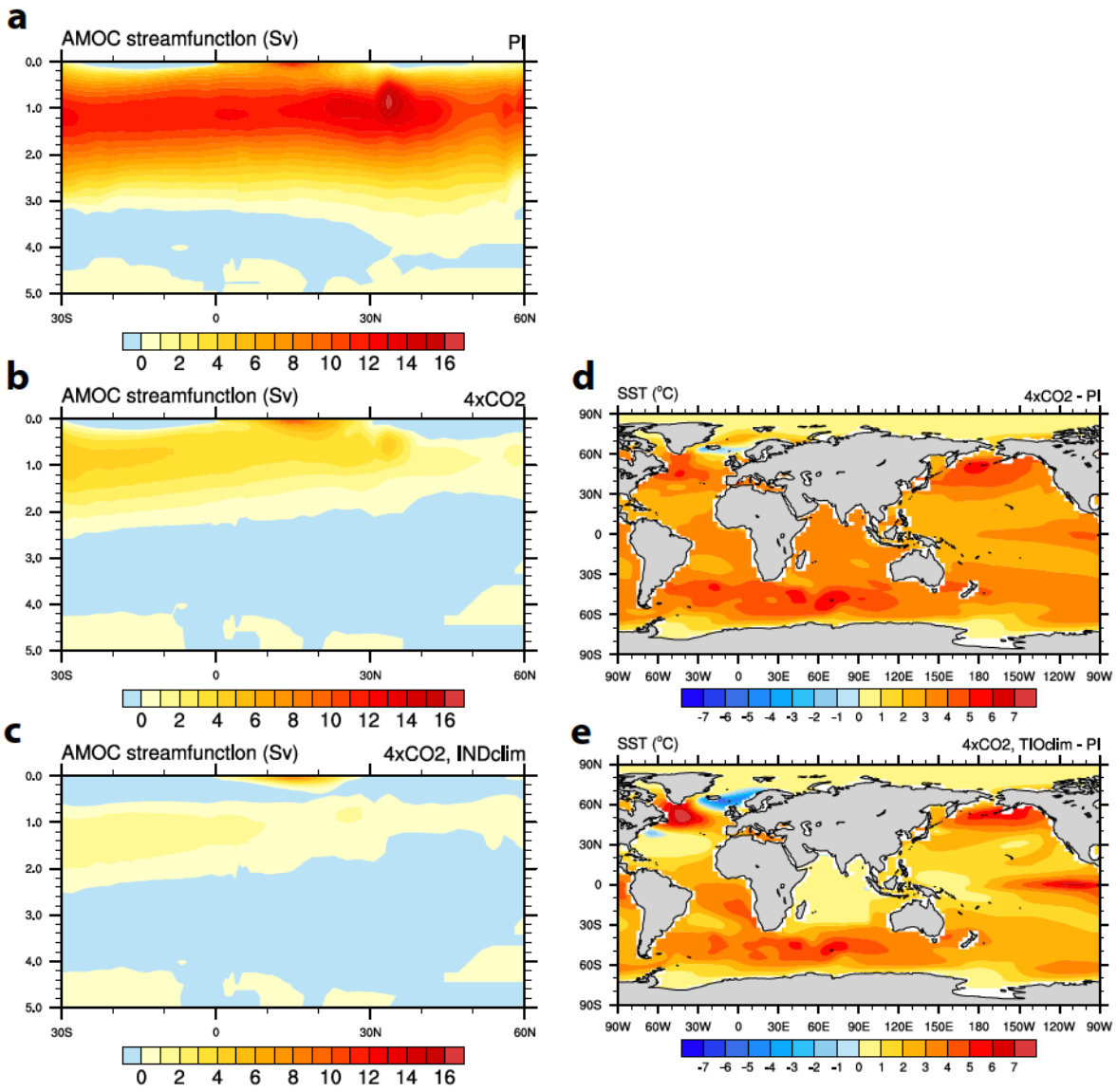

Supplementary Figure 14 | Stabilizing effect of the tropical Indian Ocean warming on the AMOC. (a-c) AMOC streamfunction in the simulations of (a) the pre-industrial state, (b) CO2 quadrupling, and (c) CO2 quadrupling with the TIO warming suppressed. (d-e) SST anomalies for the two perturbation experiments, respectively.

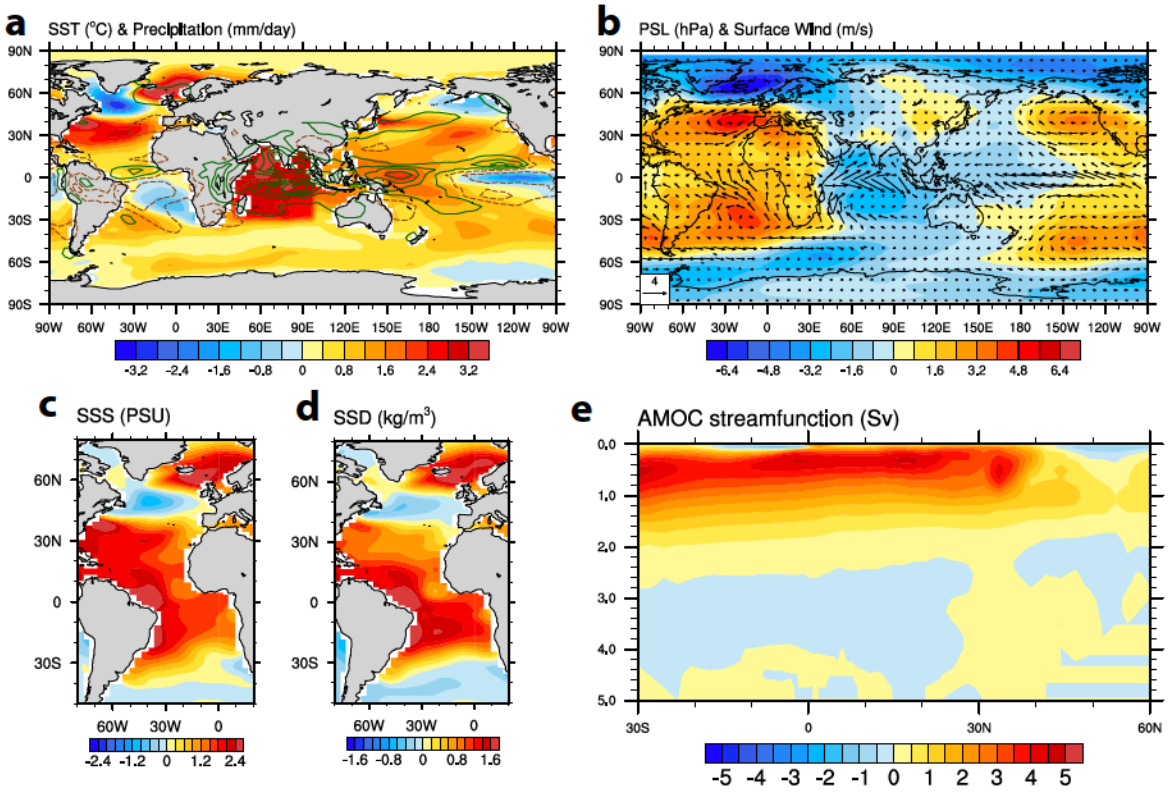

Supplementary Figure 15 | The role of tropical Indian Ocean warming under quadrupled CO_2 scenario. As in Fig. 3 but with a warming background state. Anomalies in (a) SST and precipitation (contours; 0.6 mm/day interval), (b) sea level pressure and surface wind (arrows), (c) sea surface salinity (psu), and (d) sea surface density (kg/m^3), and in (e) AMOC streamfunction, due to the TIO warming under the quadrupling of CO_2. The anomalies are computed for the last 50 years of the "4xCO2" experiment with respect to the "4xCO2,TIOclim" simulation (Methods). In panel a, the green and brown contours represent positive and negative precipitation anomalies, respectively; the contours start from the values of 0.3 mm/day and -0.3 mm/day.

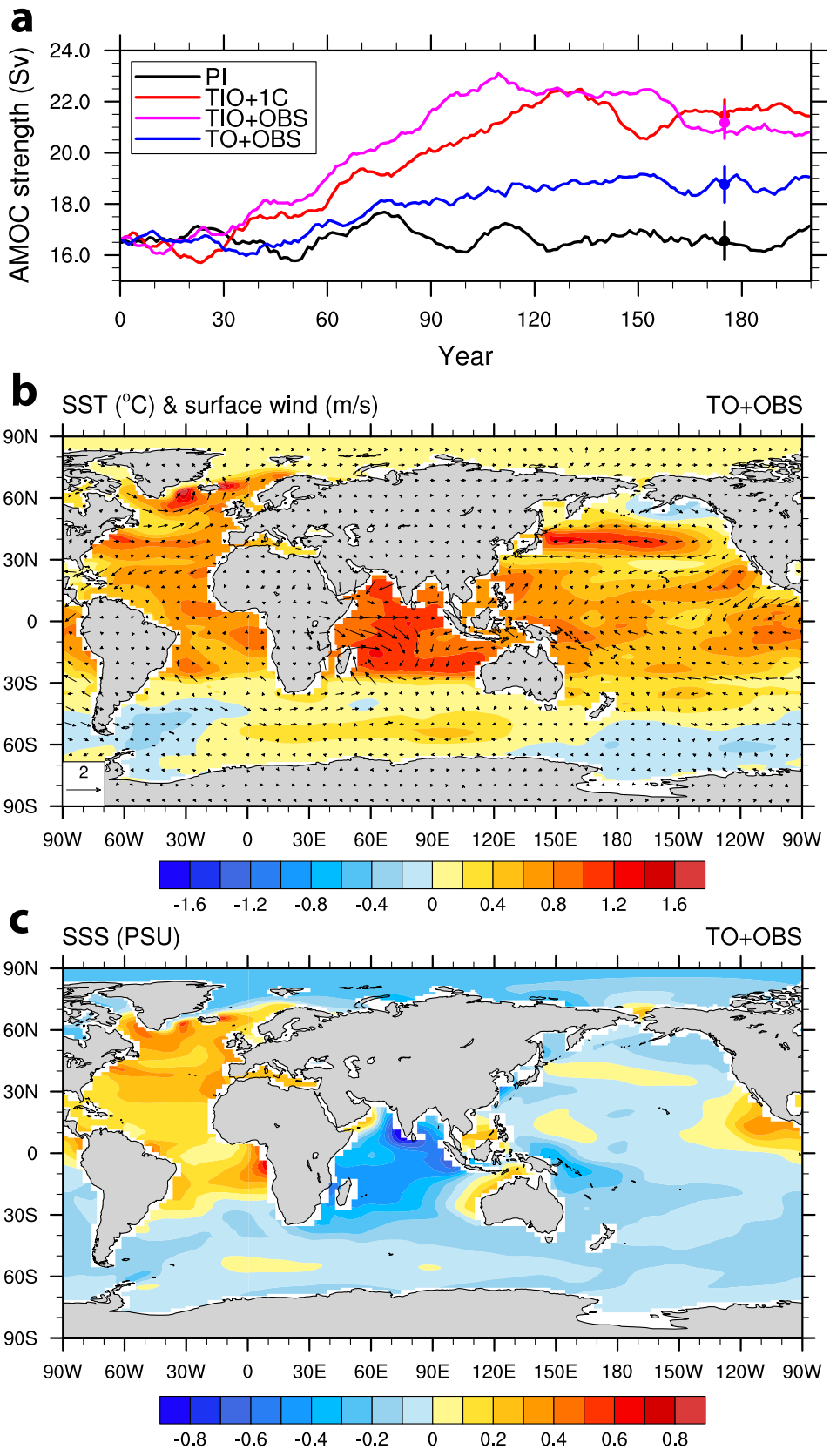
a
AMOC strength (Sv)
24.0
22.0
20.0
18.0
16.0
PI
TIO+1C
TIO+OBS
TO+OBS
0
30
60
90
120
150
180
Year
b
SST (°C) & surface wind (m/s)
TO+OBS
90N
60N
30N
0
30S
60S
90S
2
90W
60W
30W
0
30E
60E
90E
120E
150E
180
150W
120W
90W
-1.6
-1.2
-0.8
-0.4
0
0.4
0.8
1.2
1.6
c
SSS (PSU)
TO+OBS
90N
60N
30N
0
30S
60S
90S
90W
60W
30W
0
30E
60E
90E
120E
150E
180
150W
120W
90W
-0.8
-0.6
-0.4
-0.2
0
0.2
0.4
0.6
0.8

Supplementary Figure 16 | The model AMOC and climate response to the observed tropical ocean warming. (a) The evolution of AMOC intensity for the perturbation experiment wherein we imposed an SST anomaly equivalent to the observed SST trends over all tropical oceans since the 1950s ('TO+OBS'), see Methods; the pre-industrial case ('PI'), the 1°C TIO warming case ('TIO+1C'), and the experiment with an imposed SST anomaly equivalent to the SST trends over the tropical Indian ocean ('TIO+OBS') are shown for comparison. The AMOC intensity is estimated as the maximum streamfunction within 500-5500 m, 28°N-90°N. An 11-year running mean is applied to all curves. The dots and bars indicate average values and interannual variability over the last fifty years, respectively; the latter is estimated as standard deviation relative to an 11-year running mean. (b,c) The spatial patterns of the generated anomalies in (b) SST (°C) and surface winds (m/s) and (c) sea surface salinity (psu) for the TO+OBS experiment.

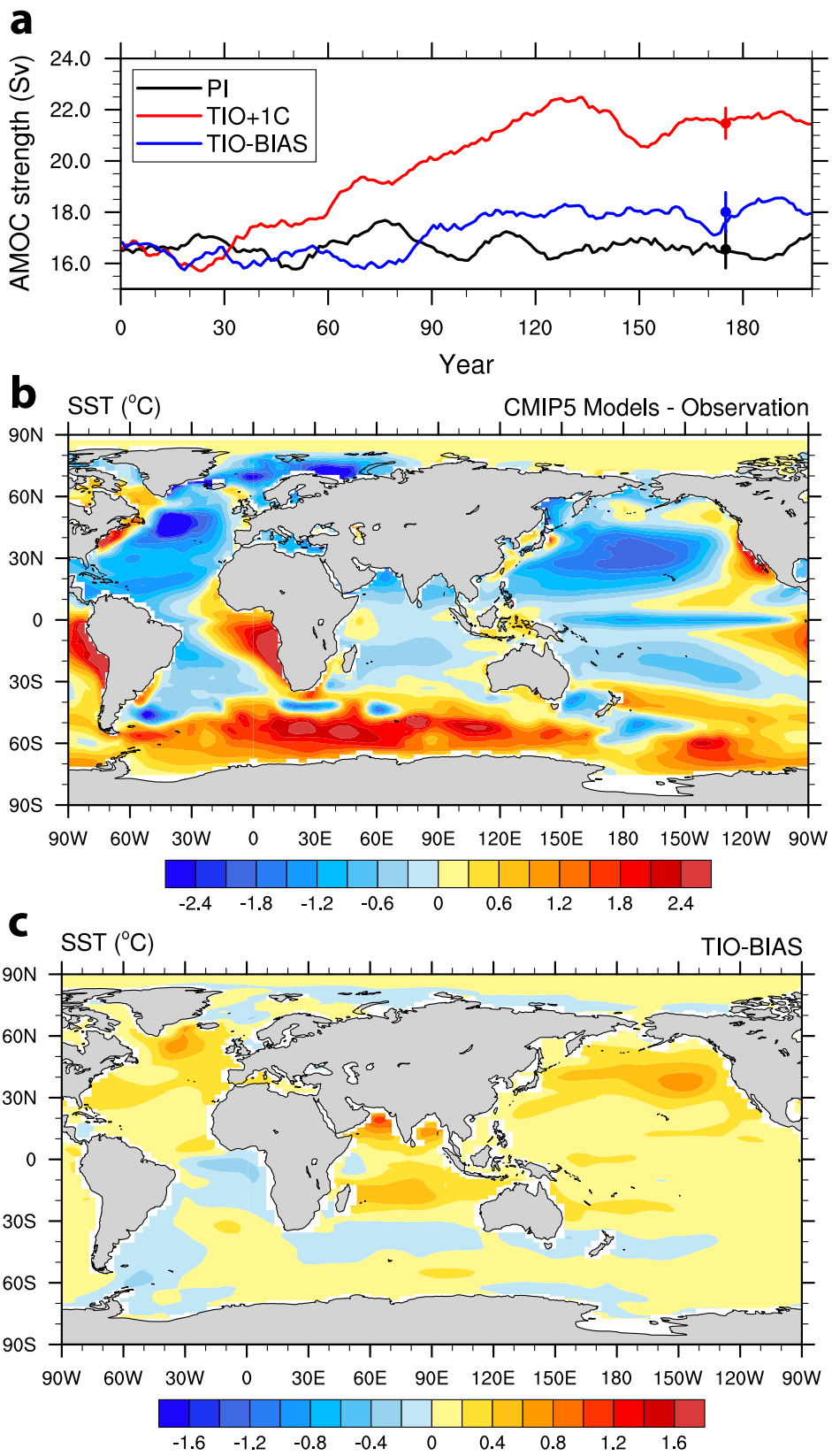
a
AMOC strength (Sv)
24.0
22.0
20.0
18.0
16.0
PI
TIO+1C
TIO-BIAS
0
30
60
90
120
150
180
Year
b
SST (°C)
CMIP5 Models - Observation
90N
60N
30N
0
30S
60S
90S
90W
60W
30W
0
30E
60E
90E
120E
150E
180
150W
120W
90W
-2.4
-1.8
-1.2
-0.6
0
0.6
1.2
1.8
2.4
c
SST (°C)
TIO-BIAS
90N
60N
30N
0
30S
60S
90S
90W
60W
30W
0
30E
60E
90E
120E
150E
180
150W
120W
90W
-1.6
-1.2
-0.8
-0.4
0
0.4
0.8
1.2
1.6

Supplementary Figure 17 | CMIP5 model bias and the tropical Indian Ocean. (a) The evolution of AMOC intensity in the perturbation experiment wherein we corrected the TIO multi-model mean cold bias present across CMIP5 ('TIO-BIAS', Methods); the pre-industrial ('PI') and the 1°C TIO warming ('TIO+1C') experiments are shown for comparison. The AMOC intensity is estimated as the maximum streamfunction within 500-5500 m, 28°N-90°N. An 11-year running mean is applied to all curves. The dots and bars indicate average values and interannual variability over the last fifty years, respectively; the latter is estimated as standard deviation relative to an 11-year running mean. (b) CMIP5 multi-model mean SST bias with respect to ERSST v4 dataset for the period of 1900-2005. (c) The response of global SST to the imposed correction to the TIO cold bias (i.e. TIO-BIAS minus PI). Note the AMOC strengthening by 1-2 Sv after year 90 and a significant warming at northern mid and high latitudes in the Pacific and Atlantic.